JOURNAL OF CATALYSIS 129, 67–87 (1991)

Solid Electrolyte Cyclic Voltammetry for *in Situ* Investigation of Catalyst Surfaces

C. G. VAYENAS, A. IOANNIDES, AND S. BEBELIS

ICE/HT and Department of Chemical Engineering, University of Patras, Patras 26110, Greece

Received August 16, 1990; revised November 21, 1990

The technique of cyclic linear potential sweep chronoamperometry, more commonly termed cyclic voltammetry, has been applied for the first time, in conjunction with on-line mass spectrometry, IR spectroscopy, and gas chromatography, to investigate the chemisorptive and catalytic properties of porous metal catalyst films also functioning as electrodes in solid electrolyte cells. The cases of O_2 adsorption and C_2H_4 oxidation on Pt were examined. It was found that solid electrolyte cyclic voltammetry (SECV), which causes a cyclic variation in catalyst work function, provides useful *in situ* information about the coverage of adsorbed species and also about the occurence of non-Faradaic electrochemical modification of catalytic activity (NEMCA effect) on the catalyst surface. The technique also permits estimation of the "length" of the catalyst–solid electrolyte–gas three-phase boundaries.

INTRODUCTION

The use of solid electrolyte cells to measure in situ the activity of oxygen on catalyst surfaces was originally proposed by C. Wagner (*1*). In this technique, first used by Vayenas and Saltsburg (*2*) and termed solid electrolyte potentiometry (SEP) (*3–5*), a porous metal catalyst film serves also as an electrode in a solid electrolyte cell. Work in this area has been reviewed recently (*6–8*). The measured cell potential can be usually related to the activity of oxygen on the catalyst surface (*2–9*). The technique is particularly useful for the study of oscillatory reactions (*3, 5, 6*) and was used to first demonstrate experimentally that rate oscillations on Pt catalyst surfaces under atmospheric pressure conditions are due to Pt oxide formation (*3, 5, 10, 11*). It has been recently shown, both theoretically and experimentally, that the potential of solid electrolyte cells provides a direct measure of the average work function difference of the gas-exposed metal surfaces of the catalyst and reference electrodes (*12* and references therein). Thus solid electrolyte cells are, essentially, work function probes (*12*).

Solid electrolyte cells with electrocatalytic electrodes can also be used for chemical cogeneration, i.e., for the simultaneous production of chemicals and power (*6, 7, 13*), and also to enhance the rate of several reactions both electrocatalytically (*14*) and catalytically (*15*). Work prior to 1988 was reviewed recently (*6, 7*).

In the course of these investigations the effect of non-Faradaic electrochemical modification of catalytic activity (NEMCA) was recently discovered (*12, 16–24*); i.e., it was found that the rate of *catalytic* reactions occuring on the gas-exposed catalyst surface of metal films deposited on solid electrolytes can be reversibly increased by up to a factor of 70 (*24*) and that this reversible steady-state catalytic rate increase can be up to 3×10^5 times higher than the rate of supply or removal of ions (such as O^{2-} or Na^+) to or from the catalyst surface (*12, 16–24*). This means that each ion (e.g., O^{2-}) supplied onto the catalyst surface can cause up to 3×10^5 chemisorbed reactant molecules or atoms to react. The term "electrochemical promotion in catalysis" was recently proposed (*25*) to describe the NEMCA effect which is reversible, appears

0021-9517/91 $3.00

to apply to all metal-catalyzed reactions (*12, 16–24*), and has revealed that the rates of metal-catalyzed reactions depend exponentially on the average catalyst surface work function (*12, 16–19, 22–24*).

The NEMCA effect has been shown to be due to the change in the binding strength of chemisorptive bonds caused by the change in catalyst surface work function (*12, 26*) which is due to the polarization of the metal–solid electrolyte interface and to the concomitant ion spillover (*16–24*). In a broad sense one can consider NEMCA to be both a remote control effect (*27*) and also an electrochemically induced and controlled Schwab effect of the second kind (*28*). The catalytic reactions for which the NEMCA effect has been studied so far (*12, 16–24*) fall into two groups, depending on whether their rates increase or decrease exponentially with increasing catalyst work function. The terms "electrophobic" and "electrophilic" have been proposed for these two groups of reactions (*12, 18, 22–24*). The Pt-catalyzed oxidation of C_2H_4 studied in the present work is a typical example of an electrophobic reaction (*12, 16, 17, 23*). Under fuel-lean conditions the rate increases exponentially with increasing work function (*17, 23*) since the rate-limiting step involves cleavage of a metal–electron acceptor (e.g., Pt–O) bond (*12, 16, 17, 23*).

The technique of cyclic voltammetry or, more precisely, linear potential sweep chronoamperometry, is used routinely in aqueous electrochemistry to study the mechanisms of *electrocatalytic* reactions (*29–31*) and also to study *ex situ* the states of catalyst surfaces (*32*). There have been some early applications of cyclic voltammetry in solid electrolyte cells with *point* electrodes at temperatures near 1000°C (*33–35*) in order to characterize the point defects associated with Cu (*33*) and Ce (*34*) dissolved in stabilized zirconia solid electrolytes and also to examine the possible electrocatalytic role of surface electron holes (*35*). No catalytic reaction was involved in these studies.

In this investigation the solid electrolyte cyclic voltammetry (SECV) technique is used with porous Pt catalyst film electrodes, one of them being exposed to a chemisorbing gas or to a reactive gas mixture and serving as a catalyst. The purpose of this investigation was two-fold: first to examine whether SECV can provide *in situ* information about chemisorbed species and second to examine if SECV can be used as a quick initial test of the NEMCA behavior of catalytic reactions. In addition to fulfilling these two initial goals the present work also shows that SECV can be used to provide an estimate for the "length" of the three-phase boundaries between the metal, the solid electrolyte, and the gas phase. This "length" is found to be proportional to the exchange current I_0 of the catalyst–electrolyte interface, which is an important parameter not only in the quantitative description of NEMCA (*12, 16–24*) but also in the field of high temperature electrocatalysis (*6*).

It is worth pointing out that, although the theory of cyclic voltammetry originally developed by Sevcik (*36*), Randles (*37*), Delahay (*38*), and Srinivasan and Gileadi (*39*) and lucidly presented by Bard and Faulkner (*29*) is very well established and understood in aqueous electrochemistry, one must be cautious when applying this theory to the solid electrolyte–catalyst systems of the type described here, as some nontrivial refinements may be necessary. The reason for this is shown schematically on Fig. 1. In aqueous electrochemistry the entire metal surface is usually *electrocatalytically* active. Even when a gas is produced or consumed, as e.g. in many fuel cell applications, there is usually a thin aqueous film covering the entire metal surface so that in most cases the charge transfer reaction occurs over the entire metal surface. Here only a small fraction of the metal surface, i.e., the fraction which is in the vicinity of the solid electrolyte–metal–gas three-phase boundaries (tpb), is electrocatalytically active and catalyzes the charge transfer reaction,

$$O(\text{tpb}) + 2e^- \rightleftharpoons O^{2-}, \qquad (1)$$

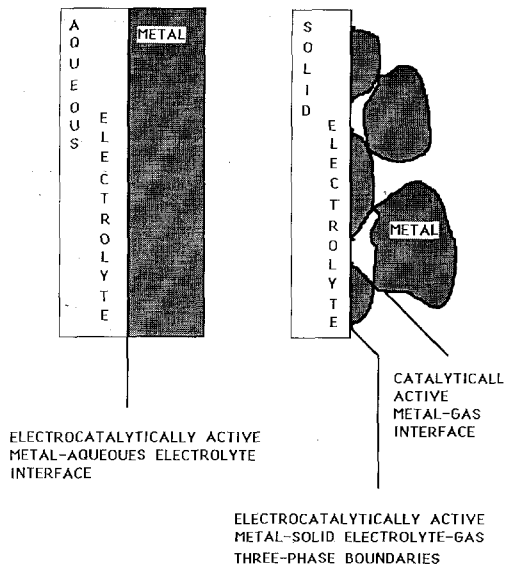

FIG. 1. Schematic representation of the location of electrocatalytically active sites in aqueous electrochemistry and of electrocatalytically and catalytically active sites in solid electrolyte electrochemistry.

where the symbol O(tpb) stands for oxygen dissociatively chemisorbed on Pt at the three-phase boundaries where oxygen ions O^{2-} are supplied to or from the O^{2-}-conducting zirconia solid electrolyte (Fig. 1). The largest fraction of the metal film surface area, typically more than 99%, is exposed to the gas phase and is only *catalytically* active (e.g., for C_2H_4 oxidation).

EXPERIMENTAL

The apparatus utilizing on-line mass spectrometry (Balzers QMG 311 with a QDP 101 data processor), IR spectroscopy (Beckman 864), and gas chromatography (Perkin–Elmer Sigma 300) is shown schematically in Fig. 2 and has been described previously (*17–23*).

The 8 mol% Y_2O_3-stabilized ZrO_2 solid electrolyte cell–CSTR reactor shown in Figs. 3 and 4 has been also described in previous papers (*5, 17–22, 42*). The three-electrode system shown in Figs. 3 and 4a was used in conjunction with a potentiostat–galvanostat (AMEL 553) and a function generator (AMEL 567). This setup permits linear variation in time of the catalyst potential V_{WR} with respect to the reference Pt/21 kPa O_2 electrode (Fig. 4b),

$$V_{WR} = V_{WR,i} + vt; \quad 0 < t \leq \tau/2 \quad (2a)$$

$$V_{WR} = V_{WR,s} - vt; \quad \tau/2 < t \leq \tau \quad (2b)$$

$$\tau = 2(V_{WR,s} - V_{WR,i})/v, \quad (2c)$$

where $V_{WR,i}$ is the initial ($t = 0$) catalyst potential corresponding to the beginning of each cycle, $V_{WR,s}$ is the switching potential, and v (V/s) is the sweep rate.

At the same time the current I flowing between the catalyst and the counter electrode is recorded, simultaneously with the rate of the catalytic reaction (in the present case C_2H_4 oxidation) taking place on the gas-exposed catalyst surface. The current I is traditionally plotted as a function of V_{WR}

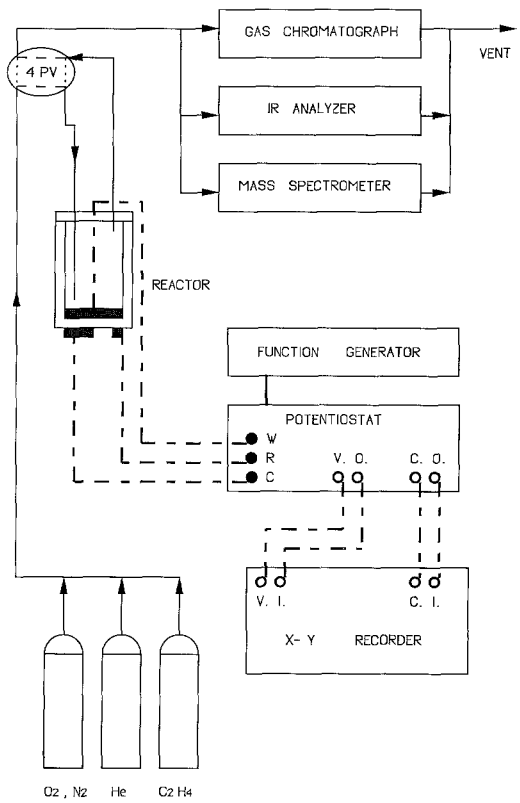

FIG. 2. Schematic diagram of the apparatus.

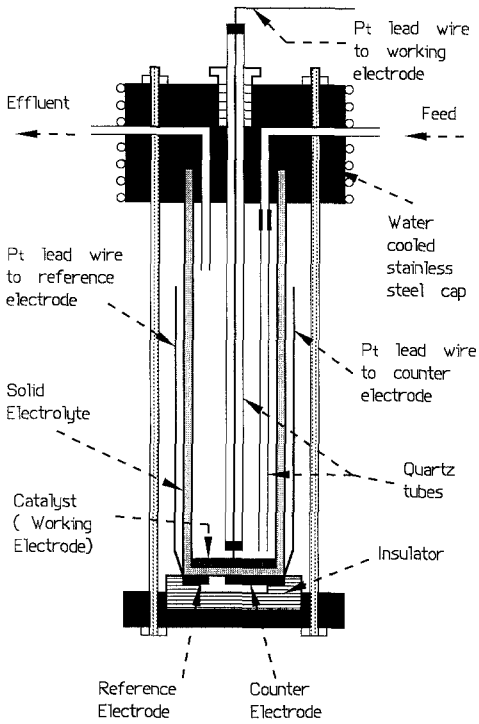

FIG. 3. Zirconia catalytic reactor.

using an $X-Y$ recorder and thus a "cyclic voltammogram" is produced. In this study, as in previous ones (*12, 16–24*), $I > 0$ corresponds to anodic currents, i.e., $I/2F$ expresses the rate of *supply* of O^{2-} *to* the catalyst surface.

It is worth pointing out that recent theoretical (*17–19*) and experimental studies utilizing a Kelvin probe (*12, 23, 40*) have shown that for solid electrolyte cells

$$eV_{WR} = \Delta e\Phi, \tag{3}$$

where $e\Phi$ is the average work function of the gas exposed catalyst surface. Equation (3) is exactly valid at steady state and approximately valid during transients (*23, 40*). Consequently the cyclic potential sweep described by Eq. (2) and depicted schematically in Fig. 4b causes a corresponding cyclic variation in the catalyst surface work function. Similarly to the case of classical cyclic voltammograms where I, and consequently the rate of the *electrocatalytic* reaction $I/2F$, is plotted vs V_{WR} on an $X-Y$ recorder, it is possible here, in view of the NEMCA effect, to obtain cyclic catalytic rate–work function graphs by plotting on an

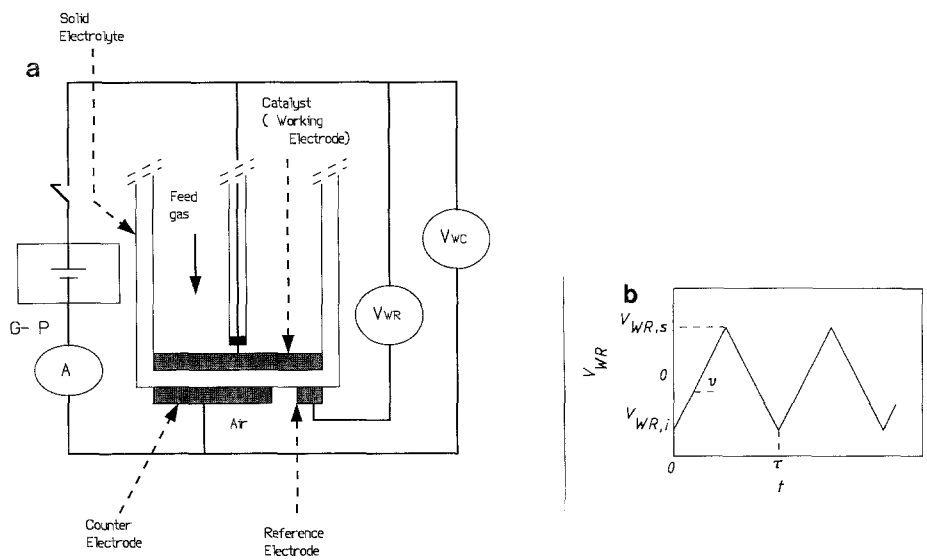

FIG. 4. (a) Electrode configuration and electric circuit; (b) imposed variation in catalyst potential V_{WR} during solid electrolyte cyclic voltammetry.

TABLE 1

Catalyst	Reactive oxygen uptake (N_O/g-atom O)	Average value of reactive oxygen uptake at the 3-phase boundaries (tpb) ($N_{O,tpb}$/g-atom O)	Exchange current density, i_0, at 400°C and P_{O_2} = 21 kPa (A/cm^2)
C_1	4.8×10^{-8}	0.17×10^{-9}	0.37×10^{-6}
C_2		0.82×10^{-9}	1.0×10^{-6}
C_3		0.62×10^{-9}	0.63×10^{-6}
C_4	3.9×10^{-9}	1.8×10^{-9}	2.0×10^{-6}
C_5		16×10^{-9}	16×10^{-6}
C_6		17×10^{-9}	18.1×10^{-6}

X–Y recorder the catalytic rate r (or turnover frequency) vs catalyst potential V_{WR} or, equivalently, catalyst work function $e\Phi$. Such a plot is presented in the Results section.

An important parameter in cyclic voltammetric studies is the sweep rate v. It was found experimentally that, for reasons explained under Discussion, the most useful information could be extracted with v values between 5 and 200 mV/s.

Porous Pt catalyst films as well as counter and reference electrodes were prepared as described previously (*5, 7, 20*), i.e., by using thin coatings of Engelhard A1121 Pt paste followed by drying and calcining in air, first for 2 h at 400°C and then for 20 min at 820°C. Scanning electron micrographs of such porous films, which are typically 5–10 μm thick, have been shown in a recent paper (*17*). *Ex situ* XPS has shown that they contain no detectable metal impurities (*5, 20*). The catalyst film is deposited on an $A = 2$ cm^2 solid electrolyte surface area. Six catalyst films were used in the course of the present investigation. The reactive oxygen uptake N_O of two of the films is shown in Table 1. The table also lists the values of the exchange current density $i_0 = I_0/A$ of the catalyst–solid electrolyte interface and additionally the value of the oxygen uptake at the three-phase boundaries, which is denoted by $N_{O,tpb}$. The procedure for measuring N_O and the exchange current I_0 is briefly outlined below. The measurement of $N_{O,tpb}$ is presented under Results.

The reactive oxygen uptake of the *entire* Pt catalyst surface N_O was measured by an isothermal surface titration technique described in detail elsewhere (*3, 5, 17, 23*). In brief, the catalyst is first exposed to O_2, then to ultrapure He for a time t_{He} at least eight times longer than the reactor residence time (2–3 s), and finally to CO or C_2H_4. The IR CO_2 analyzer is used to measure the total amount of CO_2 formed and thus the amount of chemisorbed oxygen which had remained on the surface at t_{He}. By varying t_{He} one can study the kinetics of oxygen desorption (*3, 5, 17, 23*). By extrapolating to $t_{He} = 0$ one determines N_O. The parameter N_O is a measure of the total catalyst film surface area, which is typically of the order of 30 cm^2 for the films used in this investigation.

The exchange current I_0 is extracted from standard Tafel plots as described in detail previously (*17–20, 23*) and provides a measure of the nonpolarizability of the metal–solid electrolyte interface. The parameter I_0 expresses the electrocatalytic activity of the interface for the charge-transfer reaction under consideration, e.g., reaction (1). Contrary to fuel cell applications where high I_0 values are desirable to minimize overpotential losses, it is well established that for NEMCA applications highly polarizable, i.e., low I_0 metal–solid electrolyte interfaces are required (*12, 16–24*). This is

because it is exactly the development of activation overpotential that causes NEMCA and, consequently, both theory (*17, 18*) and experiment (*12, 16–24*) have shown that the enhancement factor Λ defined from

$$\Lambda \equiv \Delta r(\text{catalytic})/(I/2F) \quad (4)$$

is, for all reactions studied so far, of the order of

$$\Lambda \approx 2Fr_o/I_0, \quad (5)$$

where r_o is the regular, i.e., open-circuit ($I = 0$) catalytic rate. For porous metal films deposited on zirconia the parameter I_0 is also expected (*16, 17, 41, 42, 46*) to be proportional to the "length" l of the metal–solid electrolyte–gas three-phase boundaries, since it is exactly at these three-phase boundaries that the *electrocatalytic* charge transfer reaction (*1*) is taking place. As shown under Results, the use of SECV enables one to measure $N_{O,tpb}$ and thus, using the atomic radius of Pt, to obtain an estimate of the three-phase boundary length l, which is extremely difficult to measure otherwise.

The SECV experiments during C_2H_4 oxidation on the gas-exposed Pt catalyst surface were carried out under the same temperature, residence time, and gas composition conditions used during the detailed investigation of the NEMCA behavior of C_2H_4 oxidation (*17*), i.e., 0.5 kPa $< P_{O_2} <$ 12 kPa, 0.1 kPa $< P_{C_2H_4} <$ 2.5 kPa, 300°C $< T <$ 400°C.

RESULTS

Voltammograms during O_2 Chemisorption

General features. Figure 5a shows a typical cyclic voltammogram of a Pt catalyst film exposed to an O_2–N_2 mixture with an oxygen partial pressure $P_{O_2} = 21$ kPa. The imposed catalyst potential waveform and resulting current response are also shown as a function of time on the same figure. Before concentrating on the main features of this voltammogram, which are the cathodic ($I <$ 0) peak labeled D and the small anodic ($I >$ 0) peak labeled B, it is worth discussing first briefly some of the overall qualitative features. For a more detailed discussion the reader is referred to the electrochemical literature (*29*).

The main reason that the current follows different paths on the V_{WR}–I plane upon increasing V_{WR} (curve ABC) and upon decreasing V_{WR} (curve CDA) is due to the fact that part of the current is used to charge the metal–solid electrolyte interface, which has a nonzero capacitance C_d. The "thickness" δI of the cyclic voltammogram (Fig. 5a) is of the order of $2vC_d$. Thus δI decreases with decreasing sweep rate v and vanishes, together with the peaks labeled D and B, for $v = 0$. In this limit the entire cyclic voltammogram collapses into a single curve between A and C, which is simply the graph of the Butler–Volmer equation (*17, 41*) for the catalyst–solid electrolyte interface,

$$I/I_0 = \exp[\alpha_a F(V_{WR} - V^o_{WR})/RT] - \exp[-\alpha_c F(V_{WR} - V^o_{WR})/RT], \quad (6)$$

where V^o_{WR} is the open-circuit ($I = 0$) catalyst potential and α_a and α_c are the anodic and cathodic transfer coefficients (*17, 18*).

Another factor which can affect the exact shape of a cyclic voltammogram is the value of the "uncompensated" resistance R_u between the catalyst and the reference electrode. This is because the charging current decays to the value vC_d, and thus the voltammogram "thickness" δI decays to the value $2vC_d$ within a time R_uC_d (*29*). Thus it is important to maintain R_u as small as possible by minimizing the distance between the catalyst and reference electrodes, i.e., by using this solid electrolyte components. In all previous NEMCA studies (*12, 16–24*) the uncompensated resistance R_u and corresponding potential drop IR_u (typically 5–30 mV) were determined via the current interruption technique in conjunction with a storage oscilloscope (*17–19, 41*). In the present study IR_u has not been subtracted from V_{WR}, since it introduces only a minor distortion in the cyclic voltammograms.

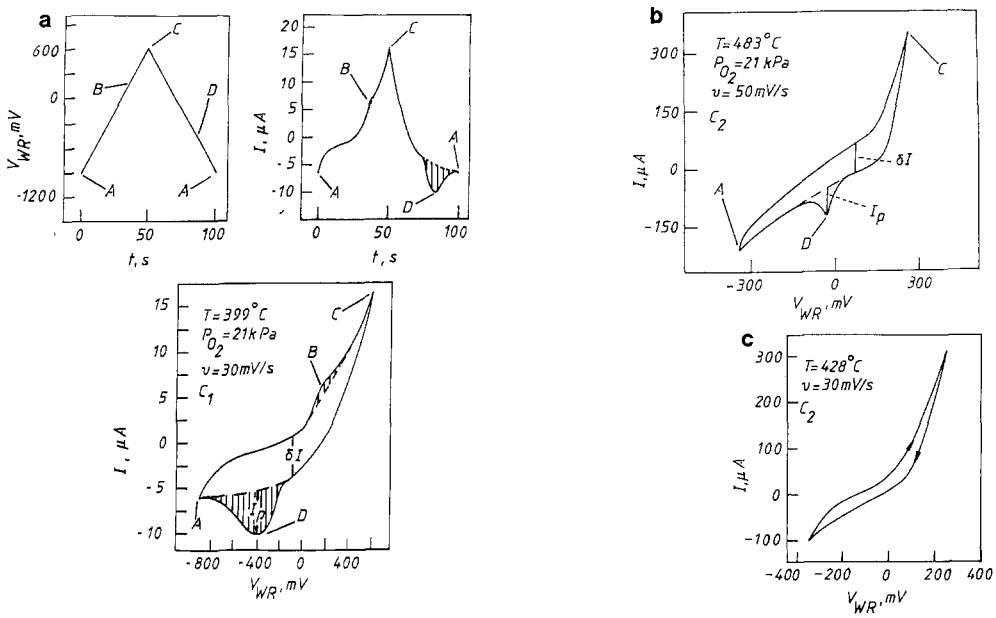

FIG. 5. Typical cyclic voltammograms of Pt films C_1 and C_2 exposed to P_{O_2} = 21 kPa (5a and 5b respectively) and of film C_2 exposed to He (5c). See text for discussion.

The peaks labeled D and B are thus the only nontrivial features of the voltammogram in Fig. 5a. The cathodic peak D centered at $V_{WR,p} = -400$ mV corresponds to the reduction of oxygen chemisorbed at the three-phase boundaries:

$$O(tpb) + 2e^- \rightarrow O^{2-}. \quad (7)$$

The shaded area of the peak on the *I–t* plane, i.e., $\int_D Idt$, is 5.1×10^{-5} C, which corresponds via Faraday's law to the reduction of $N_{O,tpb} = 2.6 \cdot 10^{-10}$ g-atom of O(tpb). This is a factor of 185 smaller than the reactive oxygen uptake $N_O = 4.8 \cdot 10^{-8}$ g-atom O of the *entire* catalyst surface. This is to be expected on the basis of Fig. 1 and of the corresponding discussion in the Introduction.

The peak height I_p of peak D (Fig. 5a) also conveys useful physical information: According to the theory of cyclic voltammetry in aqueous electrochemistry (*29*), when the electroactive species is adsorbed (i.e., O(tpb) in the present case) and the charge transfer reaction (i.e., reaction (*7*)) is "irreversible" (i.e., slow relative to O^{2-} diffusion in the electrolyte, thus not in equilibrium), then I_p is given by

$$I_p = n\alpha_c n_c F^2 \nu N_{O,tpb}/(2.72RT), \quad (8)$$

where n (=2) is the total number of transferred electrons, α_c (≈1) (Refs. (*41, 42*)) is the cathodic transfer coefficient, and n_c (=1) (Refs. (*41, 42*)) is the number of electrons transferred in the rate limiting step of the charge transfer reaction (Eq. 7). Application of Eq. 8 to the conditions of Fig. 5a gives $I_p = 9.6$ μA, which is in reasonable agreement with the experimental value of 5μA. This implies that both $\int_D Idt$ and I_p can be used for the estimation of $N_{O,tpb}$.

In order to appreciate some of the differences observed in the cyclic voltammograms of different catalyst films under different experimental conditions it is useful to compare the voltammograms of Figs. 5a and 5b. They were obtained with two catalyst films having significantly different I_0 values (Table 1). The difference in I_0 is even larger than Table 1 shows, due to the higher op-

erating temperature in Fig. 5b (I_0 = 54 μA in Fig. 5b vs 0.74 μA in Fig. 5a). There are two main differences in these two voltammograms: First, the anodic peak B (Fig. 5a) is missing in Fig. 5b. Second, the peak potential $V_{WR,p}$ of the cathodic peak D is now shifted to a significantly more positive value, i.e., $V_{WR,p} \approx -50$ mV. It is useful and important to explain both of these differences.

The anodic peak disappearance in Fig. 5b is due to the higher operating temperature and can be explained as follows: Peak B in Fig. 5a is caused by the reverse of the charge transfer reaction (7), i.e., by

$$O^{2-} \rightarrow O(tpb) + 2e^{-}. \quad (9)$$

However, even in Fig. 5a the area $\int_B Idt$ of the anodic peak B is a factor of 10 smaller than the corresponding area of the cathodic peak D. This is because reaction (9) is competing, rather unsuccessfully, with direct oxygen chemisorption from the gas phase to the three-phase boundaries,

$$\tfrac{1}{2}O_2(g) \rightarrow O(a) \rightarrow O(tpb), \quad (10)$$

where O(a) is oxygen dissociatively chemisorbed on the gas-exposed catalyst surface. Direct O(tpb) formation fromO_2(g) is also possible. Reaction (10) brings the O(tpb) coverage very near its equilibrium value under the P_{O_2} and T conditions of the experiment within a time shorter than the operating SECV time τ. The ratio ρ' of the areas of peaks B and D (Fig. 5a) provides a measure of the ratio of the rates r_9 and r_{10} of reactions (9) and (10) respectively; i.e.,

$$r_9/r_{10} \approx \rho'/(1 - \rho'). \quad (11)$$

Thus r_9/r_{10} is less than 0.1 in Fig. 5a and immeasurably small in Fig. 5b. The decrease in r_9/r_{10} with increasing T can be rationalized as follows: Although the first step in Eq. (10) is known to be weakly dependent on T, e.g. (*17*), the second step involving surface diffusion is strongly temperature-dependent (*41*c, *47*), thus peak B disappears at higher temperatures.

The positive shift of the potential peak

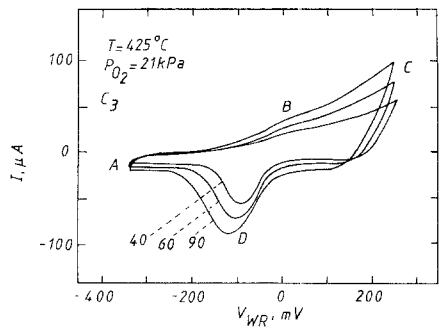

FIG. 6. Effect of sweep rate v (in mV/s) on the cyclic voltammogram of Pt film C_3 exposed to P_{O_2} = 21 kPa.

$V_{WR,p}$ (Fig. 5b vs. 5a) is mainly due to the temperature difference and to the concomitant significantly (almost thirtyfold) higher $I_0/2FN_{O,tpb}$ ($=K$) value. Indeed, lowering K is known to cause significant negative shifts to cathodic peaks (*29*). The theoretical (*29*) $V_{WR,p}$ shift of 190 mV, computed from Eq. 12.5.21 in Ref. (*29*), an activation energy of 40 kcal/mole for I_0 (*17, 41, 42*), and the K values extracted in the present study is, however, somehow smaller than the observed one.

As shown on Fig. 5c, the cathodic peak D disappears when the catalyst is exposed to pure He. Under these conditions the coverage of oxygen at the three-phase boundaries is negligible and consequently anodic currents lead to direct O_2(g) evolution.

Effect of sweep rate. Figure 6 shows the effect of sweep rate v on the cyclic voltammograms and, in particular, on the cathodic peak D. The anodic peak B is barely detectable indicating again that O(tpb) is formed primarily from O_2(g) and not from O^{2-}. Increasing v causes an almost linear increase in I_p and shifts $V_{WR,p}$ to more negative potentials. The theory of cyclic voltammetry (*29*) predicts that for the irreversible reduction of an adsorbed electroactive species it is

$$\Delta V_{WR,p} = -(RT/\alpha_c n_c F)\Delta \ln v. \quad (12)$$

The theoretically predicted shift of -48 mV upon v varying from 40 to 90 mV/s is in

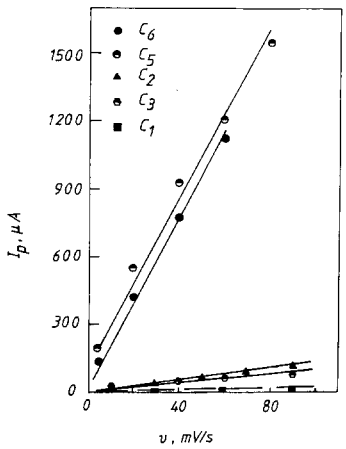

FIG. 7. Effect of sweep rate v on the maximum cathodic peak current I_p: C_1, T = 394°C; C_2, T = 483°C; C_3, T = 425°C; C_5, T = 412°C; C_o, T = 404°C. P_{O_2} = 21 kPa.

excellent agreement with the experimental value of −40 mV (Fig. 6).

The linear increase in I_p with v (Fig. 7) is also in good agreement with theory (*29*). i.e., with Eq. (8). It is worth pointing out that when the charge transfer reaction does not involve a chemisorbed reactant, then, in practically all other cases, I_p varies linearly with $v^{\frac{1}{2}}$ and not with v (*29*).

According to Eq. (8) the slopes of I_p vs v in Fig. 7 must equal $n\alpha_c n_c F^2 N_{O,tpb}/(2.72\ RT)$. Since $n = 2$, $\alpha_c = 1$, and $n_c = 1$ it follows that these slopes should equal $2F^2 N_{O,tpb}/(2.72\ RT)$. Indeed, upon comparing the $N_{O,tpb}$ values obtained from the slopes of Fig. 7 with the independently measured (via $\int_D Idt$ and also via I_p) $N_{O,tpb}$ values, one finds excellent agreement between theory and experiment. Therefore one can conclude that the slopes of I_p vs v plots can also be used for measuring $N_{O,tpb}$.

Effect of P_{O_2}. Figure 8 shows the effect of P_{O_2} on $N_{O,tpb}$ at constant T, i.e., it depicts the oxygen adsorption isotherm at the three-phase boundaries. The parameter $N_{O,tpb}$ has been computed by two different ways: First via $N_{O,tpb} = \int_D Idt/(2F)$ and second via I_p and Eq. (8). The agreement is reasonable, despite the systematic difference shown on Fig. 8. The origin of this systematic difference is not obvious. The important point, however, is that in either case a Temkin isotherm, i.e.,

$$N_{O,tpb}/N_{O,tpb,(P_{O_2}=21kPa)} = k_1 \ln(k_2 P_{O_2}) \quad (13)$$

provides an excellent fit to the data, whereas a Langmuir isotherm clearly fails, as one can easily verify by appropriately replotting the data of Fig. 8. As analyzed in the Discussion, the observation that oxygen chemisorption at the three-phase boundaries follows a Temkin isotherm provides the means for reconciling the two different physical meanings of the emf V°_{WR} of solid electrolyte cells, i.e., the fact that in addition to functioning as normal galvanic cells, solid electrolyte cells with metal electrodes are also work function probes for the gas-exposed electrode surfaces (*12, 40*).

Effect of temperature. Figures 9a and 9b show the effect of T, at constant P_{O_2}, on the cyclic voltammogram (Fig. 9a) and on the cathodic peak D only (Fig. 9b) for two different catalyst films. The behavior is almost identical. The peak size first increases, reaches a maximum near 450°C, then decreases rather abruptly and vanishes at a temperature near 570°C, which we denote by T_d. There is also a gradual positive shift of the peak potential $V_{WR,p}$ with increasing T (Fig. 9). It is interesting to note that $V_{WR,p}$ approaches zero as T_d is approached. This positive shift is due to the increase in the exchange current I_0 and K with increasing T.

A more detailed picture of the effect of T on $N_{O,tpb} = Q/2F$, where $Q = \int_D Idt$ is the cathodic peak area, is given on Fig. 10. There are four distinct temperature ranges. In the low T range, denoted by (I), $N_{O,tpb}$ increases abruptly with an apparent activation energy of 55 kcal/mole. This is followed by a more gradual increase in range (II) with an apparent activation energy of 7 kcal/mole. Then in range (III) $N_{O,tpb}$ decreases with an apparent ΔH of 22 kcal/mole, followed by a very rapid decrease in range (IV), until it vanishes at $T_d \approx$ 570°C. It is

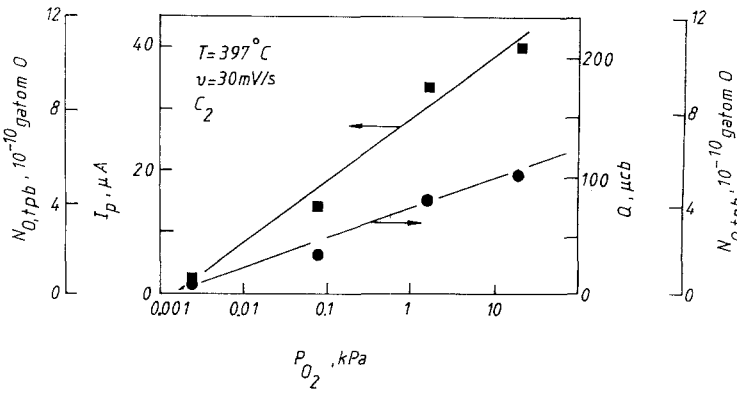

FIG. 8. Oxygen adsorption isotherm at the three-phase-boundaries computed from peak current I_p (left) and from $\int_D Idt/2F$ (right). Catalyst C_2.

worth noting on Fig. 10 that the transition temperature between ranges (III) and (IV) practically coincides with the dissociation temperature $T_{dis,1}$ of surface PtO_2 determined by Berry (*44*) whereas the dissociation temperature $T_{dis,2}$ determined by Vayenas and Michaels (*10*) lies slightly above T_d.

Figure 11 shows the effect of P_{O_2} on T_d. Increasing P_{O_2} causes an increase in T_d and, as also shown in the Figure, ln P_{O_2} varies linearly with $1/T_d$. The slope corresponds to a ΔH of, roughly, 40 kcal/mole. As previously discussed, T_d is found to be very close to the dissociation temperature of sur-

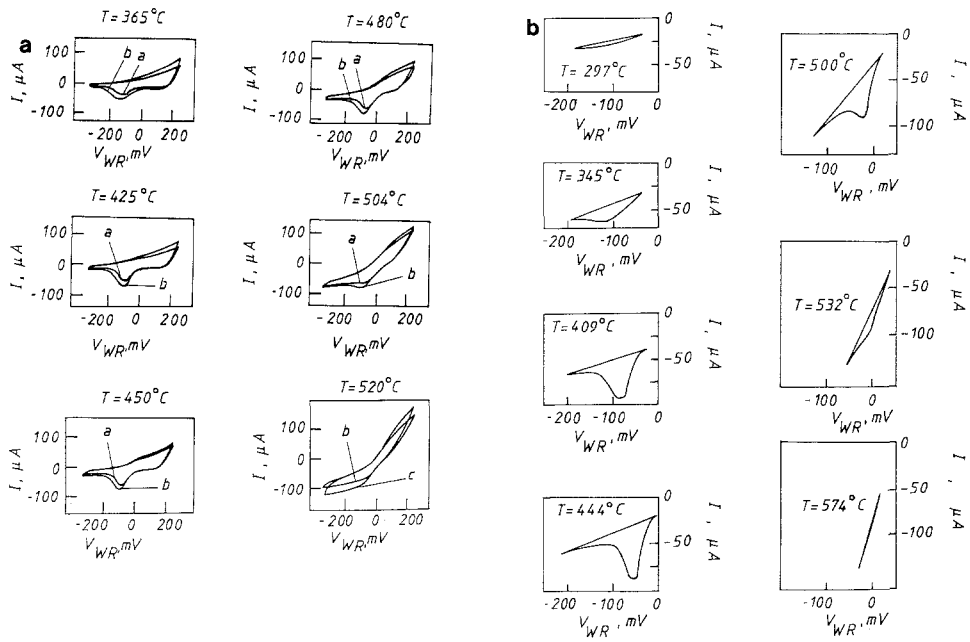

FIG. 9. (a) Effect of temperature on the cyclic voltammogram of catalyst C_3: P_{O_2} = 21 kPa; a, υ = 40 mV/s; b, υ = 60 mV/s; c, υ = 90 mV/s. (b) Effect of temperature on the cathodic oxygen reduction peak D, catalyst C_2; P_{O_2} = 21 kPa, υ = 30 mV/s.

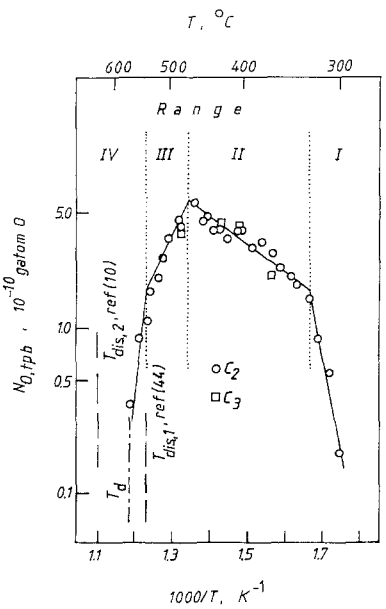

FIG. 10. Effect of temperature on the amount of oxygen adsorbed at the three-phase boundaries at P_{O_2} = 21 kPa, v = 30 mV/s.

face PtO_2 (*10*, *44*, *45*). At higher P_{O_2} and corresponding higher T_d values, agreement is better with the dissociation temperature $T_{dis,1}$ reported by Berry (*44*), while at lower P_{O_2}, T_d is closer to the dissociation temperature $T_{dis,2}$ reported by Vayenas and Michaels (*10*). The open circle in Fig. 11 shows the temperature $T_{(\theta_{O,max})}$ at which $N_{O,tpb}$ is maximized for P_{O_2} = 21kPa (cf. Fig. 10). Interestingly, this point lies very close to the isosteric line θ_O = 0.99 computed from the oxygen adsorption equilibrium constants K_O extracted by Manton (*42*) and by Yentekakis *et al.* (*5*) from electrokinetic and kinetic data on similar Pt films. The very good agreement between $N_{O,tpb}$ values for oxygen chemisorption at the three-phase boundaries and θ_O values for oxygen chemisorption on the gas-exposed catalyst surface shows that oxygen bonding at the three-phase boundaries is very similar to oxygen bonding on the gas-exposed Pt surface itself.

Dependence of I_0 on $N_{O,tpb}$. The exchange current I_0, or exchange current density $i_0 = I_0/A$, which appears in the Butler–Volmer equation (Eq. 6) is a measure of the electrocatalytic activity of the solid electrolyte–metal–gas three-phase boundaries for the charge-transfer reaction (1), i.e.,

$$O(tpb) + 2e^- \leftrightharpoons O^{2-}. \qquad (1)$$

The parameter I_0 is also a measure of the nonpolarizability of the catalyst–solid electrolyte interface. Wang and Nowick (*41*) found evidence that for porous Pt film electrodes the charge transfer reaction (1) in-

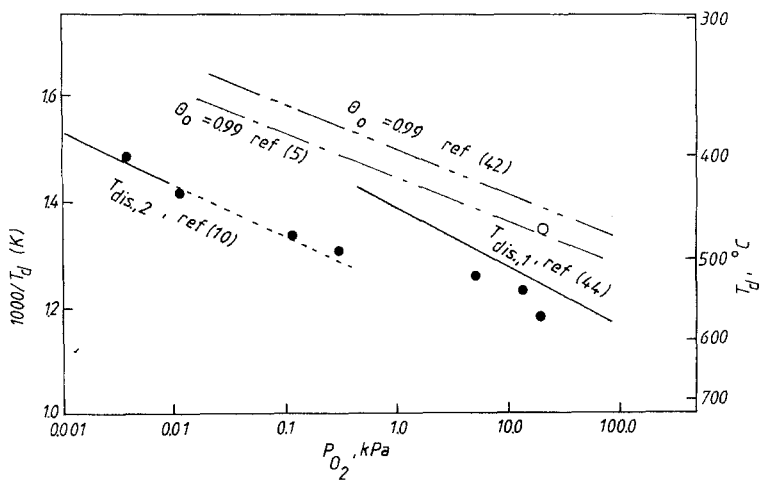

FIG. 11. Effect of P_{O_2} on T_d, catalyst C_2.

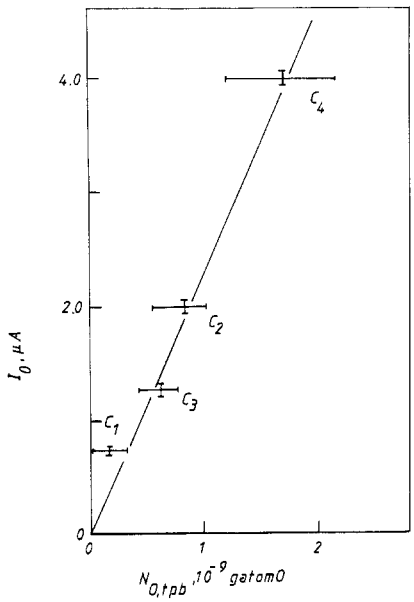

FIG. 12. Effect of maximum amount of oxygen adsorbed at the three-phase boundaries on the exchange current I_0 of the catalyst–solid electrolyte interface; T = 400°C, P_{O_2} = 21 kPa, solid electrolyte surface area A = 2 cm^2.

deed takes place at the three-phase boundaries. This is corroborated by recent results of Robertson and Michaels (*46*). Schouler and Kleitz, on the other hand, have found evidence that the electrocatalytically active zone can extend both on the electrode and on the electrolyte surface (*35*). The extent to which the metal–solid electrolyte two-phase area also participates to the charge-transfer reaction has also been the subject of investigation and dispute (*41, 46*).

The present results enable one to compare the $N_{O,tpb}$ values of different Pt catalyst films directly with the corresponding I_0 values (Fig. 12). Since I_0 is strongly temperature-dependent the comparison must be made at fixed T. The temperature T = 400°C was chosen, since near this temperature $N_{O,tpb}$ for each catalyst is close to its maximum value (Fig. 10), presumably corresponding to near complete coverage of the three-phase boundary sites. Ideally the comparison should be made not only at constant T but also at constant coverage θ_O of oxygen at the three-phase boundaries, since the latter is known to affect I_0 (*17, 41, 42*). To the extent that the comparison is made at constant T and P_{O_2}, the θ_O constancy requirement is also satisfied.

Figure 12 shows that I_0 (and, of course, i_0) is proportional to $N_{O,tpb}$. Although this result may be intuitively obvious, it is, to our knowledge, the first time that a direct experimental proof is obtained for the proportionality between electrocatalytic activity in solid electrolyte cells and reactive oxygen uptake $N_{O,tpb}$ at the three phase boundaries.

From the slope of the straight line of Fig. 12 a kinetic constant of $K = 1.25 \times 10^{-2}$ s^{-1} is extracted. It is the kinetic constant value for the charge-transfer reaction (1) under open-circuit conditions, i.e., when the rates of the forward and reverse reactions (1) are equal; K is expected to have the same temperature dependence with I_0, i.e., to increase with an apparent activation energy of 38–45 kcal/mole (*17, 41, 42*). The inverse of K provides a direct measure of the characteristic time constant of the charge transfer reaction (1).

Estimation of three-phase boundary length l. In order to compute the length l of the metal–electrolyte–gas three-phase boundaries from the measured $N_{O,tpb}$ values one must quantify the extent to which surface diffusion of adsorbed oxygen O(a) on the catalyst surface serves as a means of supplying extra oxygen O(a) to the three-phase boundaries (and converting them into O(tbp) according to the second step of reaction (10)) during the SECV operational time $\tau_0 = RT/Fv$, i.e., during the appearance of the cathodic peak D. In different terms, one must define the thickness of spreading of the electrocatalytically active zone on the Pt electrode. The thickness δ of this zone depends on the ratio of the rates of surface diffusion to the rate of the charge transfer reaction (*7*). At higher temperatures, e.g., 700°C, investigated by Robertson and Michaels (*46*), surface diffusion becomes rate

limiting and δ vanishes. However, as shown below, this is not the case for the relatively low temperatures, e.g. 400°C, used in the present study. Consequently if the effect of surface diffusion is not taken into account in computing l from $N_{O,tpb}$ gross overestimations of l will result.

The surface diffusion rate of O(a) on Pt(111) and Pt(100) was measured by Lewis and Gomer (*47*). They expressed their results as

$$D_O = \alpha^2 \nu \exp(\Delta S/R) \exp(-E/RT) \quad (14)$$

with $\alpha = 3$Å, $\Delta S = 17$ cal/(moleK), $\nu = 10^{12}$ s^{-1}, and $E = 34.1$ kcal/mole. Although this expression was obtained for relatively low O(a) averages, it is used routinely for computing the surface diffusivity of oxygen on Pt films even at high coverages (41c). From Eq. (14) one computes $D_O = 4 \times 10^{-11}$ cm^2/s for $T = 673$K, corresponding to the $N_{O,tpb}$ values of Table 1.

Using the above surface diffusivity value one can then estimate the thickness δ of the spreading zone from

$$\delta = (D_O \tau_o)^{1/2} \quad (15)$$

Using an average τ_o value of 3s one computes $\delta \approx 10^3$ Å. Using the atomic radius of Pt ($r_{Pt} = 1.4$ Å) and assuming an 1 : 1 O : Pt stoichiometry one computes that, on the average $N \approx \delta/(2r_{Pt}) \approx 360$ O(a) atoms diffuse and get reduced per three-phase-boundary electrocatalytic site during the appearance of the cathodic peak D. Consequently one can estimate l from:

$$l = N_{O,tpb} \cdot N_{Av} \cdot (2r_{Pt})(2r_{Pt}/\delta) \quad (16)$$

where N_{Av} is Avogadro's number.

The computed l value for a mean $N_{O,tpb} = 1.0 \cdot 10^{-9}$ g-atom O (Fig. 12) is $l = 470$ m. This value is in good qualitative agreement with the SEM information (*17, 48*) regarding the size, or average diameter of crystallites constituting the Pt catalyst films used in this and in previous catalytic studies on Pt/$ZrO_2(Y_2O_3)$, i.e., typically $d \approx 1$ μm. The comparison between the SEM information (*17, 48*) and the present l value can be made as follows: Assuming, for the modeling purposes, (a) that the film consists of Pt crystallites of uniform diameter d which are packed in a tetragonal arrangement and (b) that those crystallites in contact with the flat $ZrO_2(Y_2O_3)$ electrolyte are half-spheres, each with a circular πd three-phase boundary contact with the electrolyte, it follows that

$$l = \pi A/d. \quad (17)$$

Substituting $A = 2$ cm^2 and $d \approx 10^{-4}$ cm (*17, 48*), one obtains $l \approx 630$ m, in excellent agreement with the l value computed from the measured $N_{O,tpb}$ values via Eq. (16). It follows then that the measurement of $N_{O,tpb}$ in conjunction with Eq. (16) provides a reliable means for estimating l. It is worth pointing out that if the role of surface diffusion had been neglected and thus the last term $(2r_{Pt}/\delta)$ in Eq. (16) had been omitted, then the computed l values would be a factor of 360 higher. This, in conjunction with Eq. (17) would lead to $d \approx 37$ Å, i.e., a factor of 270 lower than the true experimental grain size values of 1 μm. In view of the above discussion it follows that the reactive oxygen uptake at the *true* geometric three-phase boundaries, which we denote by $N'_{O,tpb}$, is typically a factor of $\delta/2r_{Pt}$, i.e., a factor of 360 lower than the measured $N_{O,tpb}$ values.

SECV during Catalytic Reaction

General features during C_2H_4 oxidation on Pt. Figure 13a shows a typical cyclic voltammogram under reaction conditions, i.e., with the Pt catalyst exposed to an ethylene–oxygen mixture ($P_{C_2H_4} = 0.45$ kPa, $P_{O_2} = 5.3$ kPa, $T = 394$°C). The rate of CO_2 formation is monitored both by the mass spectrometer and by the IR–CO_2 analyzer. The open-circuit ($I = 0$) catalytic rate is 8.5×10^{-9} g-atom O/s and the corresponding turnover frequency (atoms O reacting/s · (surface Pt atom)) is 2.2 s^{-1}.

As shown on Fig. 13a and 13b changing V_{WR} to positive values and thus increasing the catalyst work function ($\Delta E\Phi = e\Delta V_{WR}$) induces a dramatic non-Faradaic increase in

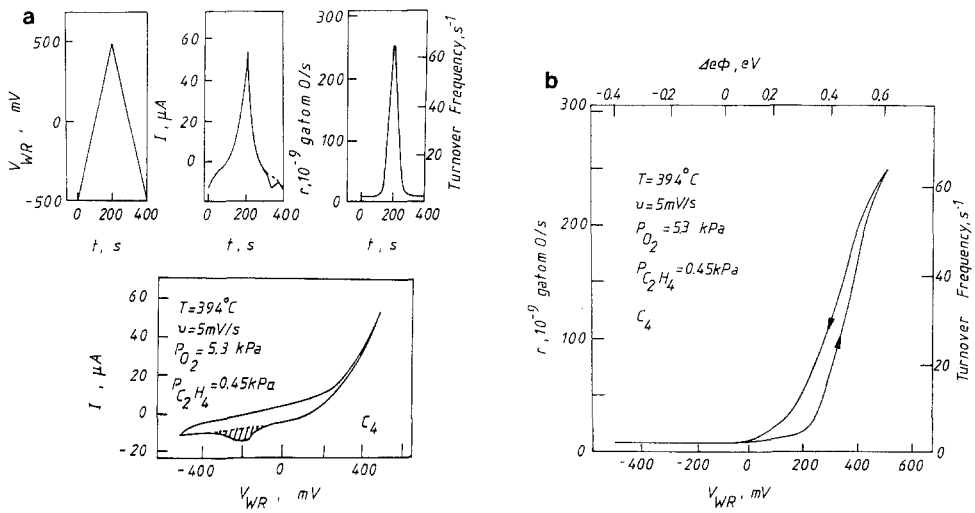

FIG. 13. (a) Solid electrolyte voltammetry (SECV) under catalytic reaction conditions: time variation of imposed catalyst potential and of resulting current I and resulting catalytic rate r and catalytic turnover frequency. The area of peak D in the cyclic voltammogram is proportional to the oxygen coverage θ_O during reaction. Catalyst C_4. (b) Cyclic variation in NEMCA induced catalytic rate and turnover frequency with catalyst potential and work function. Catalyst C_4.

catalytic rate. The maximum rate corresponds to the maximum (switching) potential $V_{WR,s}$ and is $2.5 \cdot 10^{-7}$ g-atom O/s, or equivalently expressed as a turnover frequency, 64.5 s^{-1}. Thus the rate enhancement ratio $\rho = r/r_0$ equals 29.5, while the enhancement factor $\Lambda = \Delta r/(I_{max}/2F)$, where I_{max} is the maximum current of 54 μA, equals 865.

The measured enhancement factor value ($\Lambda = 865$) is in good agreement with the value $\Lambda = 410$ predicted on the basis of the approximate expression

$$\Lambda \approx 2Fr_0/I_0 \qquad (5)$$

derived both theoretically (*17, 18*) and experimentally (*12, 16–24*) in previous studies of the NEMCA effect.

It is evident from Figs. 13a and 13b that the Pt-catalyzed C_2H_4 oxidation is an electrophobic reaction (*12, 17, 23*); i.e., the catalytic rate is enhanced with increasing catalyst potential and work function and is practically unaffected by negative currents, in excellent agreement with the detailed steady-state NEMCA studies of this reaction on Pt, with both O^{2-} conducting (*12, 17*) and Na^+ conducting (*23*) solid electrolytes.

In summary, Figs. 13a and 13b show that SECV coupled with mass spectrometry or IR spectroscopy can be used for a quick study of the NEMCA behavior of catalytic reactions. It is worth noting that even the NEMCA coefficient α, defined from (*12, 16–24*),

$$\alpha = \Delta \ln(r/r_0)/(e\Delta\Phi/k_bT) \qquad (18)$$

extracted from Fig. 13b ($\alpha = 0.5$), provides a good estimate for the published α values of this reaction (*12, 17, 23*).

It should be noted that if the cyclic plot of rate vs catalyst potential presented in Fig. 13b had been obtained with a vanishingly small scan rate υ then a single curve would have been obtained. The small hysteresis observed in Fig. 13b is mainly due to the finite time ($2FN_O/I$) required for ion spillover over the entire catalyst surface and thus for establishing the potential-work function equality (Eq. 3).

It is worth noting that the cathodic oxygen reduction peak D is also present under reac-

tion conditions (Fig. 13a), although the area $\int_D Idt$ is smaller than $(\int_D Idt)_{max}$ in the absence of ethylene, in which case the coverage θ_O of oxygen on the catalyst surface is near unity at this temperature (*3, 17*). It is thus possible to estimate the coverage θ_O under reaction conditions from

$$\theta_O = (\int_D Idt)/(\int_D Idt)_{max}. \qquad (19)$$

The thus computed θ_O value for the conditions of Fig. 13a is $\theta_O = 0.92$, in excellent agreement with the values ($\theta_O = 0.87$–0.97) computed for the same temperature and gas composition from Eq. (22) in Ref. (*3*) and also from kinetic constant values in Ref. (*3*) or (*17*). Thus one can conclude that SECV permits an *in situ* measurement of oxygen coverage on the catalyst surface under reaction conditions.

In a separate series of experiments the alternative technique of cyclic current reversal chronoamperometry (CCRC) (*29*) was employed. In this technique the current between the catalyst and the counter electrode is varied linearly while V_{WR} and the catalytic rate during C_2H_4 oxidation are monitored. Under similar conditions the same qualitative trends with SECV were observed (*49*). Detailed results are presented elsewhere (*49*). In the case of CCRC, significant complications appear often in the V_{WR} vs t and r vs t curves, which can be related to the steady state multiplicity observed on the I–V_{WR} plane during C_2H_4 oxidation on Pt (*17, 49*).

DISCUSSION

Main results. (1) Solid electrolyte cyclic voltammetry (SECV) coupled with on-line gas analysis techniques (e.g., mass spectrometry, IR spectroscopy) can provide a quick and reliable initial test for the electrophobic or electrophilic character of catalytic reactions. Thus SECV is a valuable tool for investigating the NEMCA effect (*12, 16–24*). We note that cycling the catalyst potential or, equivalently (*12, 24*) the work function could also be an attractive method for improving the time-averaged product selectivity of catalytic reactions. Work in this area is currently in progress (*43*).

(2) The use of SECV permits measurement of $N_{O,tpb}$, i.e., of the amount of electrocatalytically active oxygen in the vicinity of the three-phase boundaries of zirconia–catalyst–gas. By taking into account the role of surface diffusion on the Pt electrode one can use $N_{O,tpb}$ to estimate the geometric three-phase-boundary length. The measurement of $N_{O,tpb}$ can be made by three different, and essentially independent, methods, of which the first is entirely independent from the other two:

a. From the integral $\int_D Idt$

b. From the cathodic peak height I_p and Eq. (8)

c. From the slope of I_p vs v plots and Eq. (8).

The present results have established that $N_{O,tpb}$ is proportional to the exchange current I_0 of the catalyst–solid electrolyte interface. This shows that, at least for porous catalyst electrodes of the type used here and in previous studies of NEMCA (*12, 16–24*), the electrocatalytic reaction (1) takes place at the three-phase boundaries. This is also supported by the recent results of Robertson and Michaels (*46*), who worked at higher temperatures. However, when the metal electrode is not very porous, i.e., under "blocking electrode" conditions, the charge-transfer reaction at the Pt–ZrO_2 two-phase boundaries may be important (*41*). In fact that is probably supported even by the present results for the case of the low three-phase-boundary catalyst C_1 (Fig. 12), in which case I_0 deviates significantly from the straight line correlation with $N_{O,tpb}$. Finally, the role of oxygen adsorbed on the solid electrolyte itself may be important in some systems (*35*).

(3) The use of SECV can provide *in situ* information about the coverage of adsorbed species, e.g., oxygen, on metal films both in the presence of chemisorbing species, e.g. $O_2(g)$, and also under reaction conditions. By varying the partial pressure of the chemi-

sorbing gas one can easily obtain adsorption isotherms. Strictly speaking these isotherms refer to adsorption at the three-phase boundaries. However, the present results show that, at least for the case of oxygen chemisorption on Pt films deposited on stabilized ZrO_2, oxygen chemisorption at the three-phase boundaries is very similar energetically to oxyen chemisorption on the gas-exposed Pt catalyst surface itself. Measured θ_O values during C_2H_4 oxidation are in good agreement with previous studies (*3, 17*).

(4) The theory of cyclic voltammetry which has been developed for aqueous electrolyte systems (*29, 36–39*) is applicable with minor modifications to SECV. This is manifested, for example, by the very good fit which Eqs. (8) and (12) provide to the present data. Also, as shown in Results, all the observed general features of the voltammograms during O_2 chemisorption, including the effect of sweep rate, can be adequately described on the basis of existing theory (29). The effects of P_{O_2} and temperature, however require some additional discussion.

Oxygen chemisorption and cell emf. The fact that oxygen chemisorption at the three-phase boundaries follows a Temkin isotherm (Fig. 8) provides the means for reconciling the two different physical meanings of the emf V^{o}_{WR} of solid electrolyte cells (*12, 40*). Thus, in the absence of other chemisorbing or reacting gases and with both electrodes (working, i.e., catalyst and reference) made of the same material the Nernst equation must be satisfied under open-circuit conditions, i.e.,

$$V^{o}_{WR} = (RT/4F)\ln(P_{O_2,W}/P_{O_2,R}), \quad (20)$$

where $P_{O_2,W}$ and $P_{O_2,R}$ are the oxygen partial pressures on the catalyst and reference electrodes respectively. However, as recently shown both theoretically (*17–19*) and experimentally (*12, 40*), the quantity eV^{o}_{WR} must also equal the difference in the work function $e\Phi$ of the gas-exposed electrode surfaces, i.e.,

$$eV^{o}_{WR} = e\Phi_W - e\Phi_R. \quad (21)$$

In order to compare Eqs.(20) and (21) one must define the oxygen adsorption isotherm over the gas-exposed catalyst surface. As already shown and as further discussed below, oxygen adsorption at the three-phase boundaries and at the gas-exposed catalyst surface are energetically very similar. In fact $N_{O,tpb}$, which obeys a Temkin isotherm (Fig. 8), is the amount of atomic oxygen adsorbed not only at the geometric three-phase boundaries but also on a fairly thick zone on the catalyst surface. Thus one can reasonably assume a Temkin isotherm for the entire gas-exposed catalyst surface as well, i.e.,

$$\theta_O = k_1 \ln(k_2 P_{O_2}). \quad (22)$$

It can be shown (*43*) that upon combining Eqs. (20), (21), and (22) one obtains

$$\Delta e\Phi_W = (eRT/4Fk_1)\theta_O, \quad (23)$$

which is formally identical to the Helmholz equation

$$\Delta e\Phi_w = (eP_oN_{Pt}/\varepsilon_o)\theta_O, \quad (24)$$

where P_o is the dipole moment of oxygen chemisorbed at the catalyst surface, N_{Pt} is the surface Pt concentration, and $\varepsilon_o = 8.85 \times 10^{-12}$ C^2/J · m (23, 40). In different terms, when P_o is not strongly coverage dependent, the Temkin isotherm is the *only* isotherm which can satisfy simultaneously the Nernst equation (*20*), the Helmholz equation (*24*), and the solid electrolyte emf-work function equation (*21*). Furthermore, from the experimentally determined value of k_1 it is possible to combine Eqs. (23) and (24) and thus obtain the dipole moment P_o value. These points will be analyzed in detail in a future paper (*43*).

Temperature effect on the cathodic O (tpb) reduction peak. There are two aspects of the observed behavior (Figs. 9, 10) which need to be explained: The gradual shift of peak potential $V_{WR,p}$ to more positive potentials with increasing T (Fig. 9) and the ob-

served peak height or area variation with increasing T (Fig. 10). The former can be easily explained on the basis of the cyclic voltammetry theory for irreversible charge transfer reactions (*29*): Increasing T causes a substantial increase in I_0 and in the corresponding $K(=I_0/2FN_{O,tpb})$ value with an activation energy of the order of 40 kcal/mole (*17, 41, 42*). This is well established to cause significant positive shifts to cathodic peaks (*29*). Physically this is because increasing K and I_0 accelerates the charge transfer reaction and thus makes the peak "less irreversible" by shifting the peak potential $V_{WR,p}$ closer to its equilibrium location, i.e., $V^{o}_{WR} = (RT/4F)\ln(P_{O_2}/0.21)$.

The observed variation in peak area and height, or, equivalently $N_{O,tpb}$, with increasing T (Figs. 9 and 10) can be explained as follows: In the low temperature range (*I*) the exchange current I_0 is very small, thus the charge transfer reaction

$$O(tpb) + 2e^- \rightarrow O^{2-} \qquad (7)$$

is very slow, and consequently only a small fraction of O(tpb) formed during each cycle from O_2(g) can react within the time of "electrochemical attack" (*29*) $\tau_o = RT/Fv$. The high apparent activation energy in range (*I*) (Fig. 10) is due to the strong exponential dependence of I_0 on T (*17, 41, 42*). Thus the peak height in range (*I*) is dictated by electrokinetic considerations, i.e., by the kinetics of the charge-tranfer reaction (*7*).

In range (II) the exchange current I_0 has become sufficiently large so that practically all chemisorbed O(tpb) formed during each cycle can react according to reaction (*7*). The peak height is then dictated by the amount of O(tpb) formed during each cycle, which is dictated by the rate of the first step of oxygen adsorption in Eq. (*10*), which is only weakly activated and thus only moderately temperature dependent (*17*). Thus in range (II) the cathodic peak height is dictated by the oxygen adsorption kinetics.

In range (III) the kinetics of oxygen adsorption have become sufficiently fast that thermodynamic equilibrium is established during each cycle between O(tpb) and gaseous oxygen. Consequently $N_{O,tpb}$ starts to decrease with increasing T and the slope of $\ln N_{O,tpb}$ vs $1/T$ is near the the heat of adsorption of oxygen at the three-phase boundaries or, almost equivalently, on the gas-exposed Pt surface. The computed value (2×22 kcal/mole = 44 kcal/mole O_2) is in good agreement with values reported for oxygen chemisorption on Pt at finite coverages (*5, 41, 42* and references therein). Consequently the decrease of peak height with increasing T in range (III) is dictated by the thermodynamics of oxygen adsorption. Thus, stricktly speaking, oxygen adsorption isotherms of the type shown in Fig. 8 should be obtained in this range only. However, due to the weak temperature dependence of $N_{O,tpb}$ in range (II), such measurements can also be extended in range (II) without introducing significant experimental error.

The observed abrupt decrease in $N_{O,tpb}$ with increasing temperature once the dissociation temperature of surface PtO_2 (*10, 44, 45*) is reached, i.e., in range (IV) (Fig. 10) is, at first, surprising. In view of Fig. 10 and of the surface PtO_2 literature (*10, 44, 45*) it follows that below $T_{dis,1}$ or $T_{dis,2}$ surface PtO_2 formation is thermodynamically possible; thus the measured $N_{O,tpb}$ corresponds to oxygen chemisorbed on an already partly oxidized surface. One then would expect that as the oxide is removed by increasing T above the dissociation temperature of PtO_2, $N_{O,tpb}$ will increase, as more surface area becomes available for oxygen chemisorption at the three-phase boundaries. However, exactly the opposite happens as the cathodic peak D abruptly disappears. One might be tempted on the basis of this observation to associate the cathodic peak D with the reduction of the oxide itself. However, then it is not possible to explain the observed exponential decrease in $N_{O,tpb}$ in range (III): Contrary to chemisorbed oxygen, the equilibrium coverage of which can only decrease with increasing T, the surface concentration of an oxide can only increase, kinetically, with increasing T as long as its

dissociation temperature is not exceeded. The observed behavior in range (IV) can be explained as follows: Above the PtO_2 dissociation temperature the oxide decomposes and the resulting clean Pt surface has a much higher electrocatalytic activity than the oxidized surface (*42*) for the O(tpb) reduction step (*7*). This has been shown to be the case by steady-state I vs V_{WR} measurements (*42*). Consequently reaction (*7*) or, equivalently, reaction (*1*) has a very short time constant τ_e which is much shorter than the used operating time, or time of "electrochemical attack" (*29*), $\tau_0 = RT/Fv$, of the cyclic voltammetric technique (typically 3 s). As explained in the last section, physical or chemical processes with time constants significantly shorter than τ_0 are at steady state and thus create no peaks on the cyclic voltammogram. Therefore the cathodic peak D disappears once the dissociation temperature of PtO_2 is exceeded. In order to observe the peak above $T_{dis,1}$ or $T_{dis,2}$ one would have to use much higher sweep rates v. In this case, however, as explained in the last section, other processes such as O^{2-} diffusion to the three-phase boundaries would interfere. A corollary of the proposed explanation is that most of the activation overpotential associated with the charge-transfer reaction (*7*), or (*1*), at low temperatures is associated with the presence of PtO_2. This view is strongly supported by steady-state electrokinetic measurements (*42*).

In summary the cathodic peak height in ranges (I), (II), and (III) is dictated by electrokinetic (I), catalytic (II), and thermodynamic (III) considerations respectively, while in range (IV) the peak height decreases abruptly due to the very fast kinetics of the charge-transfer reaction (*1*) on the reduced Pt surface.

Characteristic time constants for SECV. For future applications of SECV it is important to identify, as in the case of aqueous systems, the relevant important time constants and dimensionless groups, the values of which determine if for a given system a proper cyclic voltammogram will be obtained conveying the desired information. For example the choice of exchange current I_0 (which is to a large extent controllable by the sintering temperature during catalyst preparation), operating temperature, and sweep rate will dictate in general

a. If the cyclic voltammogram will provide information about the catalyst (which is the desired case here) or about the solid electrolyte.

b. If observable peaks will be obtained and whether these peaks will be reversible (i.e. $V_{WR,p}$ related to some specific activity value via the Nernst Equation) or irreversible.

Table 2 lists the main characteristic time constants which dictate the nature of information provided by a solid electrolyte cyclic voltammogram. The table also gives typical values that these parameters had in the present study. These time constants can be grouped conceptually as following:

a. Electrocatalytic time constant τ_e. This is the time constant for the charge transfer reaction (*1*) and is equal to K^{-1}. In the present study τ_e was typically of the order of 80 s at 400°C and, since it is inversely proportional to I_0, τ_e is expected to decrease exponentially with increasing T with an apparent activation energy of about 40 kcal/mole (*17, 41, 42*).

b. Gas adsorption and catalytic time constants τ_{ad} and τ_c. The oxygen adsorption time constant τ_{ad} equals $(K_{ad}y_{O_2})^{-1}$, where K_{ad} is the oxygen adsorption kinetic constant and y_{O_2} is the oxygen mole fraction. On the basis of previously published values of K_{ad} (*3, 17*) one computes τ_{ad} to be of the order of 0.01 s at 400°C. The catalytic time constant for C_2H_4 oxidation τ_c is the inverse of the turnover frequency. It is typically of the order of 0.5 s at 400°C under open circuit conditions and decreases to 1.5×10^{-2} s under NEMCA conditions.

c. NEMCA time constant τ_N. This is the time constant for ion spillover onto the en-

TABLE 2

Characteristic Time Constants

Symbol	Definition	Typical values	Ref.
τ_e	$1/K = 2FN_{O,tpb}/I_0$	80 s	(p)
τ_{ad}	$1/K_{ad}y_{O_2}$	2×10^{-2} s	(*3*, *17*)
τ_c	N_O/r	$0.5–1.5 \times 10^{-2}$ s	(*3*, *17*, p)
τ_N	$2FN_O/I$	30–80 s	(*16–23*, p)
τ_D	$(N_{O,tpb}/AC_O)(RT/FDv)^{1/2}$	10^{-3} s	(p)
τ_{SD}	δ_f^2/D_O	1.5×10^3 s	(p)
τ_o	RT/Fv	3 s	(p)
τ	$2(V_{WR,s} - V_{WR,i})/v$	30 s	(p)

Note. (p): present work.

tire catalyst surface and has been shown (*12*, *16–24*) to equal $2FN_O/I$. In the present work τ_N is typically of the order of 30–80 s.

d. Ion diffusion time constant τ_D. The characteristic time constant τ_D for ion diffusion in the electrolyte can be defined (*29*) from $\tau_D = (N_{O,tpb}/AC_O)(RT/FDv)^{1/2}$, where C_O and D are the bulk concentration and diffusivity of O^{2-} in the solid electrolyte, respectively. In the present work τ_D was typically of the order of 10^{-3} s.

The ratio $\lambda = \tau_D/\tau_e$, first introduced by Ayabe (*29*, *50*), dictates whether a peak will be reversible ($\lambda \gg 1$) or irreversible ($\lambda \ll 1$). Computed λ values in the present work were typically of the order of 10^{-5}, indicating that indeed the O(tpb) reduction peak is clearly irreversible, in good agreement with the experimentally observed shift of $V_{WR,p}$ with sweep rate v.

e. Chemisorbed oxygen O(a) surface diffusion time constant τ_{SD}. When this quantity refers to the entire catalyst film, it can be defined from $\tau_{SD} = \delta_f^2/D_O$, where δ_f is the maximum diffusion length on the Pt film from its top to the three-phase-boundaries. On the basis of the tetragonally-packed spherical crystallite model described under Results one can compute δ_f from $\delta_f = \pi d r_{Pt}^2 N_O N_{Av}/(2A)$. Substituting $d = 1$ μm, $A = 2$ cm^2, and a mean N_O value equal to 2.6×10^{-8} g-atom O (Table 1), one obtains $\delta_f = 2.4$ μm, in very good agreement with SEM information (*17*, *48*). Thus δ_f is roughly a factor of 24 larger than the "spreading" thickness δ ($\approx 10^3$ Å) of the electroactive zone at 400°C. One thus computes that τ_{SD} is on the order of 1.5×10^3 s. The fact that τ_{SD} is significantly longer than τ_e implies that surface diffusion is relatively slow in relation to the charge transfer reaction and also to the SECV operational time τ_o. Consequently, in general, only a small fraction of the total oxygen adsorbed on the catalyst surface can participate to the charge transfer reaction. Nevertheless this fraction is not negligible for the computation of l from $N_{O,tpb}$ as discussed previously.

f. Operational time constants τ_o and τ. In aqueous cyclic voltammetry (*29*) the operational or "electrochemical attack" time constant τ_o is defined from $\tau_o = RT/Fv$. All electrocatalytic and charge transfer phenomena with time constants significantly shorter than τ_o will be at steady state and will not cause a peak in the cyclic voltammogram. Typical τ_o values in the present study were of the order of 3 s. Since in the present work catalytic phenomena are also taking place throughout the voltammogram cycle it is useful to also define an operational time constant τ from Eq. (2c), i.e., $\tau = 2(V_{WR,s} - V_{WR,i})/v$. As shown in Table 2 typical τ values employed in the present study were on the order of 30 s.

It follows from the above discussion and

from Table 2 that with τ and τ_o values used in the present study it is $\max(\tau_D, \tau_{ad}, \tau_c) \ll \tau, \tau_o < \min(\tau_N, \tau_e, \tau_{SD})$ and, consequently, the adsorptive, catalytic and ion diffusion processes are at steady state during SECV. The electrocatalytic reaction (7) is not at steady state below T_d and this is why the oxygen reduction peak appears and the electrocatalytic kinetics can be followed by SECV. Also the NEMCA induced ion spillover is not quite at steady state during the cyclic voltammograms and this gives rise to the hysteresis loop in Fig. 13b. Finally surface diffusion is slow but does allow for a finite "spreading" of the electrocatalytically active zone, a fact which must be taken into account in computing the three-phase boundary length.

CONCLUSIONS

Solid electrolyte cyclic voltammetry can be used in conjunction with on-line gas analysis techniques to study the NEMCA behavior of catalytic reactions, to obtain *in situ* information about the coverage of oxygen on metal catalyst films, and to measure the amount of electrocatalytically active oxygen at the catalyst–solid electrolyte–gas three-phase boundaries. The present exploratory study has identified some of the advantages and limitations of this new technique and has established some criteria for the rational selection of scan rate values to be employed in future studies.

ACKNOWLEDGMENTS

Financial support by the VW Foundation of the Federal Republic of Germany and by the EEC Non-Nuclear program is gratefully acknowledged. We also thank Professor C. Lamy for a helpful discussion.

REFERENCES

1. Wagner, C., *Adv. Catal.* **21,** 323 (1970).
2. Vayenas, C. G., and Saltsburg, H. M., *J. Catal.* **57,** 296 (1979).
3. Vayenas, C. G., Lee, B., and Michaels, J. N., *J. Catal.* **66,** 36 (1980).
4. Stoukides, M., and Vayenas, C. G., *J. Catal.* **74,** 266 (1982).
5. Yentekakis, I. V., Neophytides, S., and Vayenas, C. G., *J. Catal.* **111,** 152 (1988).
6. Vayenas, C. G., *Solid State Ionics* **28–30,** 1521 (1988).
7. Lintz, H.-G., and Vayenas, C. G., *Angew. Chem.* **101,** 725 (1989); Int. Engl. Edn. **28,** 708 (1989).
8. Stoukides, M., *Ind. Eng. Chem. Res.* **27,** 1745 (1988).
9. Vayenas, C. G., *J. Catal.* **90,** 371 (1984).
10. Vayenas, C. G., and Michaels, J. N., *Surf. Sci.* **120,** L405 (1982).
11. Vayenas, C. G., Georgakis, C., Michaels, J. N., and Tormo, J., *J. Catal.* **67,** 348 (1981).
12. Vayenas, C. G., Bebelis, S., and Ladas, S., *Nature (London)* **343,** 625 (1990).
13. Vayenas, C. G., and Farr, R. D., *Science* **208,** 593 (1980).
14. Gür, T. M., and Huggins, R. A., *Science* **219,** 967 (1983).
15. Stoukides, M., and Vayenas, C. G., *J. Catal.* **70,** 137 (1981).
16. Vayenas, C. G., Bebelis, S., and Neophytides, S., *J. Phys. Chem.* **92,** 5083 (1988).
17. Bebelis, S., and Vayenas, C. G., *J. Catal.* **118,** 125 (1989).
18. Neophytides, S., and Vayenas, C. G., *J. Catal.* **118,** 147 (1989).
19. Vayenas, C. G., Bebelis, S., Neophytides, S., and Yentekakis, I. V., *Appl. Phys. A* **49,** 95 (1989).
20. Yentekakis, I. V., and Vayenas, C. G., *J. Catal.* **111,** 170 (1988).
21. Vayenas, C. G., Bebelis, S., and Neophytides, S., *in* "New Developments in Selective Oxidation" (G. Genti and F. Trifiró, Eds.), pp. 643–652, Studies in Surface Science and Catalysis, Elsevier, Amsterdam, 1990.
22. Vayenas, C. G., and Neophytides, S., *J. Catal.*, in press (1991).
23. Vayenas, C. G., Bebelis, S., and Despotopoulou, M., *J. Catal.*, in press (1991).
24. Vayenas, C. G., Bebelis, S., Yentekakis, I. V., Tsiakaras, P., and Karasali, H., *Platinum Met. Rev.* **34**(3), 122 (1990).
25. Pritchard, J., *Nature (London)* **343,** 592 (1990).
26. Boudart, M., *J. Amer. Chem. Soc.* **74,** 3556 (1952).
27. Weng, L. T., Patrono, P., Sham, E., Ruiz, P., and Delmon, B., *in* "New Developments in Selective Oxidation" (G. Genti and F. Trifiró, Eds.), pp. 797–806, Studies in Surface Science and Catalysis, Elsevier, Amsterdam, 1990.
28. Boudart, M., and Djéga-Mariadassou, G., "Kinetics of Heterogeneous Catalytic Reactions," Princeton Univ. Press, Princeton, NJ, 1984.
29. Bard, A. J., and Faulkner, L. R., "Electrochemical Methods: Fundamentals and Applications," Wiley, New York, 1980.
30. Beden, B., Kadirgan, F., Lamy, C., and Leger, J. M., *J. Electroanal. Chem.* **142,** 171 (1982).
31. Papoutsis, A., Leger, J.-M., and Lamy, C., *J. Electroanal. Chem.* **234,** 315 (1987).

32. Lamy-Pitara, E., Lghouzouani, L., Tainon, Y., and Barbier, J., *J. Electroanal. Chem.* **260,** 157 (1989).
33. Fabry, P., and Kleitz, M., *J. Electrochem. Soc.* **126**(12), 2183 (1979).
34. Olmer, L. J., Viguie, J. C., and Schouler, E. J. L., *Solid State Ionics* **7,** 23 (1982).
35. Schouler, E. J. L., and Kleitz, M., *J. Electrochem. Soc.* **134**(5), 1045 (1987).
36. Sevcik, A., *Collec. Czech. Chem. Commun.* **13,** 349 (1948).
37. Randles, J. E. B., *Trans. Faraday Soc.* **44,** 327 (1948).
38. Delahay, P., "New Instrumental Methods in Electrochemistry," Interscience, New York, 1954.
39. Srinivasan, S., and Gileadi, E., *Electrochim. Acta* **11,** 321 (1966).
40. Ladas, S., Bebelis, S., and Vayenas, C. G., *Surf. Sci.,* in press (1991).
41. Wang, D. Y., and Nowick, A. S., *J. Electrochem. Soc.* (a) **126**(7), 1155 (1979); (b) **126**(7), 1166 (1979); (c) **128**(1), 55 (1981).
42. Manton, M., Sc. D. Thesis, Massachusetts Institute of Technology, 1986.
43. Vayenas, C. G., and Bebelis, S., in preparation.
44. Berry, R. J., *Surf. Sci.* **76,** 415 (1978).
45. Peuckert M., and Ibach H., *Surf. Sci.* **136,** 319 (1984).
46. Robertson, N. L., and Michaels, J. N., *J. Electrochem. Soc.* **137**(1), 129 (1990).
47. Lewis, R., and Gomer, R., *Surf. Sci.* **12,** 157 (1968).
48. Farr, R. D., and Vayenas, C. G., *J. Electrochem. Soc.* **127,** 1478 (1980).
49. Ioannides, A., Ph.D. Thesis, University of Patras, 1991.
50. Matsuda, H., and Ayabe, Y., *Z. Elektrochem.* **59,** 494 (1955).